Angular Power Distribution and Mean Effective Gain of Mobile Antenna in Different Propagation Environments

Kimmo Kalliola[1], Kati Sulonen[2], Heikki Laitinen[3], Outi Kivekäs[2], Joonas Krogerus[1], Pertti Vainikainen[2], *Member, IEEE*

[1]Nokia Research Center, Radio Communications Laboratory
[2]Helsinki University of Technology, Radio Laboratory
[3]VTT Information Technology

Abstract – We measured the elevation angle distribution and cross-polarization power ratio of the incident power at the mobile station in different radio propagation environments at 2.15 GHz frequency. A novel measurement technique was utilized, based on a wideband channel sounder and a spherical dual-polarized antenna array at the receiver. Data was collected along over 9 km of continuous measurement routes, both indoor and outdoor. Our results show that in NLOS situations the power distribution in elevation has a shape of a double-sided exponential function, with different slopes on the negative and positive sides of the peak. The slopes and the peak elevation angle depend on the environment and base station antenna height. The cross-polarization power ratio varied within 6.6 and 11.4 dB, being lowest for indoor, and highest for urban microcell environments. We applied the experimental data for analysis of the mean effective gain (MEG) of several mobile handset antenna configurations, with and without user's head. The obtained MEG values varied from approximately –5 dBi in free space to less than –11 dBi beside the head model. These values are considerably lower than what is typically used in system specifications. The result shows that considering only the maximum gain or total efficiency of the antenna is not enough to describe its performance in practical operating conditions. For most antennas the environment type has little effect on the MEG, but clear differences exist between antennas. The effect of user's head on the MEG depends on the antenna type, and on which side of the head the user holds the handset.

I. INTRODUCTION

The gain of a mobile handset antenna is a critical parameter in cellular network design. Due to the large variety of mobile phones used in the networks, it is very important that their antenna performance can be evaluated reliably. The traditional definition of antenna gain is not adequate for evaluating the performance of a handset antenna, whose orientation relative to the direction and polarization of the incident field is unknown. Several

methods have been proposed for determining the performance of a mobile antenna in realistic propagation conditions.

The random-field measurement (RFM) method [1-4] is based on measuring the mean received power level of the antenna on a random route in a typical operating environment. The mean effective gain (MEG) of the antenna is obtained as the ratio of the mean signal levels of the test antenna and a reference antenna. The effect of the user holding the handset on the antenna gain can be easily analyzed with this method [5,6]. The method is naturally closest to realism, but it is time consuming, since the repeatability of the measurements is poor, and statistical significance can only be achieved by doing extensive measurements in all possible operating environments. The RFM method can be simplified by using a field simulator to produce an artificial scattering environment in an indoor facility [7,8]. This makes the measurements repeatable, but it is not evident that the conditions resemble a realistic operating environment.

In [9], Taga derived a general expression for MEG. Using the formulas presented in [9], the MEG of an antenna in a certain environment can be computed based on the 3-D gain pattern of the antenna and the average angular distribution of incident power in the environment. The power distribution must be known in both azimuth and elevation, and separately for horizontally (ϕ-) and vertically (θ-) polarized field components. Also the cross-polarization power ratio (XPR) is needed in the calculation.

The clear benefit of the computational method for determining the MEG is that it is fast and repeatable. In addition to [9], it has been used in [4,5,10]. Currently the drawback is that there is little information available of realistic field distributions in different environments. From the random orientation of the mobile antenna in azimuth it is straightforward to assume that the azimuth distribution of the waves is uniform. Instead, no straightforward assumption can be justified for the distribution in elevation. Few published results exist on measured elevation power distributions [9,11,12]. Only [9] proposes a parameterized model for the distribution and gives the model parameters fitted to experimental data at 900 MHz, but is limited to urban macrocell environment with large base station antenna height. Another model was proposed in [13], but no measurement data was given to verify or tune the model.

In this contribution we present experimental results of the elevation power distribution (EPD) and XPR at the mobile antenna in different radio environments at 2.15 GHz frequency. The measurements were performed using a wideband radio channel sounder and a spherical dual-polarized antenna array. The measurement method,

described in [14], enables the full 3-D measurement of the spatial radio channel in real time, and thus the acquisition of large amounts of data. We compare two parameterized models for the EPD: the symmetrical Gaussian function proposed by Taga [9], and the asymmetrical general double-exponential function. We also present the fitted parameter values of both models for each measurement environment.

In addition, we apply the experimental results for MEG calculations of several practical mobile antenna configurations, with both measured and simulated radiation patterns. We consider the dependence of the MEG on the usage environment, and compare the MEG of a handset antenna to the total efficiency, gain, and cross-polarization discrimination of the antenna configuration. Furthermore, we investigate the deviation of the MEG values caused by using the model EPDs instead of the measured.

II. Mean Effective Gain

According to Taga [9], the MEG of an antenna can be expressed using the 3-D power gain pattern of the antenna and the angular power density functions of radio waves in a multipath environment, both defined separately for the θ- and ϕ-polarized[1] field components. Also the cross-polarization power ratio, i.e. the ratio of the mean incident θ- and ϕ-polarized powers along a random route in the case of θ-polarized transmission [9], is needed in the computation of MEG. The angular power density functions $p_\theta(\theta,\phi)$ and $p_\phi(\theta,\phi)$ need to satisfy the following condition:

$$\int_0^{2\pi}\int_{-\pi/2}^{\pi/2} p_\theta(\theta,\phi)\cos\theta d\theta d\phi = \int_0^{2\pi}\int_{-\pi/2}^{\pi/2} p_\phi(\theta,\phi)\cos\theta d\theta d\phi = 1 \quad (1)$$

The spherical coordinate system is defined in Fig. 1. It should be noted that according to (1) the definition of the angular power density functions differs from that of the joint probability density function for the direction of arrival $f(\theta,\phi)$, defined in [15], which satisfies:

$$\int_0^{2\pi}\int_{-\pi/2}^{\pi/2} f(\theta,\phi)d\theta d\phi = 1 \quad (2)$$

[1] θ and ϕ polarizations correspond to the vertical and horizontal polarizations used in [9] in the plane perpendicular to the incidence angle

It follows by combining (1) and (2) that the relation between the angular power density function and joint probability density function for the direction of arrival is:

$$p(\theta,\phi)=\frac{f(\theta,\phi)}{\cos\theta} \tag{3}$$

It is natural to assume that when a mobile user moves randomly in any environment, the incident waves can arise from any azimuth direction with equal probability. If the power density function in azimuth is uniform and independent of elevation, the joint angular power density functions reduce to:

$$p(\theta,\phi)=\frac{1}{2\pi}p(\theta) \tag{4}$$

In contrast to the azimuth, no straightforward assumption can be justified for the power distribution in elevation. Previously few models have been presented. The first model by Clarke [16] assumes that all energy is concentrated in the horizontal plane. However, it is known to be unrealistic at least in urban environments, where buildings give rise to multipath components from high elevation angles. Aulin [17], proposed a generalization of Clarke's model to a case where all energy does not travel in the horizontal plane, but no data was available to verify the model. Also reference [13], which proposes a family of functions to describe the power distribution in elevation, lacks measurement data. In [9], Taga proposed the Gaussian density function, and fitted the parameters to experimental data. However, he used only four measured points of the elevation power distribution, which is not necessarily sufficient to verify the distribution.

III. Description of Experiments

A. Measurement Setup

We measured the angular power distribution separately for θ- and ϕ-polarized components of the incident field at the mobile station in different propagation environments using the measurement method presented in [14]. The method is based on a spherical array of 32 dual-polarized antenna elements, and a complex wideband radio channel sounder. At the base station (BS), a wideband signal was transmitted using a single fixed vertically

polarized antenna. At the mobile station (MS), the signal was received separately from the θ- and ϕ-polarized feeds of each of the 32 elements of the spherical array, using a fast 64-channel RF switch. Approximately five snapshots[2] of the received signal were sampled and stored per each wavelength the mobile moved, except for the highway macrocell environment, where the number of snapshots per wavelength was between two and three. The center frequency was 2.154 GHz and the carrier was modulated by a PN-sequence with 30 MHz chip frequency. Detailed information of the used HUT/IDC channel sounder can be found in [18].

During the measurements the transmitting antenna was placed in fixed locations corresponding to typical BS antenna installations in different cellular radio network configurations. A modified commercial GSM1800 sector antenna with 10 dBi gain and 3 dB beamwidth of 80° in azimuth and 28° in elevation was used in all cases except for the indoor picocell, where the transmitting antenna was omnidirectional (vertical 3 dB beamwidth 80°, gain 2 dBi). It must be noted that the radiation pattern of the transmitting antenna affects the power distribution at the receiver. The transmitting antennas were chosen as typical examples of BS antennas used in existing networks at cell configurations similar to the measured ones, to obtain as realistic results as possible.

B. Processing of Data

The delays, directions-of-arrival (DoAs), amplitudes, and phases of both θ- and ϕ-polarized components of the incoming waves at each measurement snapshot were found through sequential delay-domain and angular-domain processing. First the received signal of each antenna feed was correlated with a replica of the transmitted PN-sequence to obtain the complex impulse response of the channel. The delay taps were then identified by detecting the local maxima of the power delay profile averaged over the array elements. Corresponding to each delay tap, there may exist one multipath component or several components separated by their DoAs. Up to four multipath components per delay tap were estimated using the beamforming scheme with pre-computed array weights (2° beam spacing in azimuth and elevation), as described in [14]. Only such multipaths were accepted whose amplitude exceeded a threshold value of 6 dB below the highest multipath, in order to filter out spurious signals due to sidelobes of the array. The measured sidelobe level of the array is approximately −10 dB in the case of two simultaneous multipaths [14], but the level increases with an increasing number of multipaths.

[2] one PN sequence period from all 64 channels

The amplitudes and phases of the θ- and ϕ-polarized components of the incident waves were obtained by pointing θ- and ϕ-polarized beams in these directions. As a final result, we had for each measurement snapshot the angle resolved impulse response, defined as:

$$\begin{bmatrix} h_\theta(\theta,\phi,\tau) \\ h_\phi(\theta,\phi,\tau) \end{bmatrix} = \sum_{l=1}^{L} \begin{bmatrix} \alpha_{\theta,l} \\ \alpha_{\phi,l} \end{bmatrix} \delta(\theta-\theta_l)\delta(\phi-\phi_l)\delta(\tau-\tau_l) \tag{5}$$

where h_θ and h_ϕ denote the θ- and ϕ-polarized components of the impulse response, respectively. $\alpha_{\theta,l}$ and $\alpha_{\phi,l}$ are the complex amplitudes of l^{th} multipath, θ_l and ϕ_l are the corresponding elevation and azimuth angles, and τ_l is the delay.

The total spatial resolution of the measurement is determined by the angular resolution of the spherical array of approximately 40° and the 33 ns delay resolution of the wideband channel sounder. Thus the spatially separable blocks are truncated cones with an opening angle of 40° and length of 10 m, and the size of the block increases with increasing distance between the last scattering point and the array. The azimuth and elevation power distributions for θ- and ϕ-polarized wave components were derived from the angle resolved impulse response using formulas presented in Table 1. First the instantaneous power vs. incidence angle was computed as a sum of the multipath powers. Then the mean relative power vs. incidence angle in one environment was obtained by averaging over all snapshots in the environment. The variation of the received power due to large scale fading was compensated by normalizing the result to the total incident power at each point. Due to the large measurement bandwidth compared to the channel coherence bandwidth the fast fading of the total received power (sum of the multipath powers) was small. The distribution of the square root of the total power agreed well with Rice distribution and the average fitted Rice factor varied from k≈17 in the outdoor-indoor case to k≈60 in the urban macrocell case. Finally the azimuth (APD) and elevation power distributions (EPD) were obtained from the mean relative powers vs. incidence angle as presented in Table 1.

C. Measurement Environments

We performed measurements in five different radio environments. The environments, the approximate total route lengths, and the numbers of collected snapshots are presented in Table 2. Also the percentages of line-of-sight (LOS) and non-line-of-sight (NLOS) measurements are shown. The characteristic features of each environment

are briefly described below. In all measurements except of those of the highway macrocell the spherical array acting as the mobile station was mounted on a trolley, where the center of the array was at height of 1.7 m above ground level and the visible arc in elevation was from zenith to approximately −60°.

The indoor picocell measurements were carried out in the transit hall of Helsinki airport. The omnidirectional BS antenna was elevated at 4.6 m above the floor level and located so that the visibility over the hall was good. The BS−MS distance varied from 10 to 150 m. The portion of LOS measurements was significant, of the order of 40 %.

The outdoor−indoor measurements were performed in two different office buildings, both having four floors, and office rooms next to the outer walls made of brick. In both sites the BS antenna was placed on the rooftop of the neighboring building. The average distance from BS to the mobile routes was in the range of 50 to 100 m. The short distance was forced by the limited sensitivity of the measurement due to the losses in the switching unit. The BS antenna was approximately 3 and 8 m above the mobile antenna for the two sites. The measurement routes include both corridors and office rooms, and the ceiling height is in the range of 2.5 to 3 m in both buildings.

The urban micro- and macrocell measurements were performed in the center of Helsinki, Finland. The spherical array was located on a trolley, and the routes were driven along the sidewalks of the streets. Fig. 2 presents a map showing the BS positions and the measured mobile routes. The street grid in the measurement area is fairly regular and the average street width is approximately 15 m. The height of most buildings is in the range of 20 to 30 m.

In the microcell environment the same mobile routes were measured for the same base station location with three different BS antenna heights. The antenna was located on the sidewalk of a street, and mounted on a person lift elevated at 3, 8, and 13 m above the street level. The main beam of the antenna pointed west along the street. The measurement routes included the main street with LOS to the BS, the two parallel streets on both sides, and four transversal streets in front of the antenna (see Fig. 2). The BS−MS distance varied from 10 to 350 m.

In the urban macrocell measurements the BS antenna was located on the rooftop of a parking house and pointed separately to two opposite directions in order to cover larger area (see Fig. 2). The antenna heights from ground were 27 and 21 m, the former being at, and the latter above the rooftop level of the opposite buildings. Photographs showing the views from both macrocell antenna installations can be found in [19]. The BS−MS

distance varied from 50 to 750 m. Due to the limited sensitivity of the measurement system we were not able to measure propagation distances corresponding to the radii of biggest urban macrocells. However, our measurement distances are in line with many current urban site configurations in cellular networks today.

The highway macrocell measurements were carried out in an industrial area in Espoo, Finland. The BS antenna was located on top of a building next to a junction of a ring road with a lot of traffic. Few large buildings exist in the area, and for most of the routes only trees obstruct the direct LOS path. The BS antenna height was 17 m. The measurement routes included the transversal ring road, and the crossing road. The BS–MS distance varied from 50 to 1200 m. In these measurements the spherical array was mounted inside a person car, on the front seat, and at the height of the passenger's head (1.3 m). It must be noted that the metallic chassis of the car has a significant effect on the angular distribution and polarization of the electric field at the antenna inside the car. However, it is common nowadays to use mobile handsets inside vehicles, which makes this a practical scenario.

IV. Angular Distribution of Incident Power

A. Experimental Azimuth Power Distribution

When a mobile antenna moves along a random route, uniform distribution is the only reasonable assumption for the power distribution in azimuth. However, to illustrate the radio propagation in urban environment, we present two examples of measured power distributions in different environments. Fig. 3 shows the APD in urban microcell (h_{BS} = 3 m) and urban macrocell environments. It can be seen that the distributions are not at all uniform, but that some directions are more probable than others. This is due to the fact that the measured mobile routes are not random in nature, but that they are parallel and perpendicular to street canyons (see Fig. 2). In the microcell case, Fig. 3 (a), highest maxima are produced in directions close to 0° and 180°, i.e. the directions of the street canyon along which the mobile is moving. The third maximum at left (90°) is due to propagation via crossing streets. The routes were by chance chosen so that the BS is almost always at left-hand side when looking to the moving direction of the mobile. If this had not been the case, the obtained azimuth power distribution would have four maxima with angular separation of 90°. In the macrocell case, Fig. 3 (b), the APD is closer to uniform than in the microcell, but the left hand side of the distribution (angles 0°...+180°) clearly dominates. As in the microcell, the reason for this is that the routes were not random. However, since a real mobile user may turn around or cross the streets at any angle, uniform distribution is the only justified

assumption for the azimuth power distribution averaged over a *random* route in any environment. Fig. 3 shows that both in urban micro- and macrocell cases the differences between the θ- and ϕ-polarized distributions are small.

B. Experimental Elevation Power Distribution

In contrast to the azimuth, it seems obvious that the elevation power distribution depends on the environment type as well as on the BS antenna height and BS–MS distance. Fig. 4 presents the mean relative power vs. elevation angle in different environments. Also the average of all distributions is presented. The figure demonstrates that the EPD depends on the environment and BS antenna height. In all environments dominated by NLOS channels the shape of the EPD is similar for angles close to horizontal plane: the power decays roughly exponentially on both sides of the peak of the EPD, until approximately 1 % of the peak power. Both the slope of the exponential decay and the shape of the EPD outside the main lobe depend on the environment. It should be noted, though, that in all environments most of the power is concentrated in small positive elevation angles. This is in agreement with measurements by Lee and Brandt [20], who showed that most of the power is concentrated in elevation angles lower than 16° above horizontal level.

In the indoor picocell measurements significant portion of the mobile routes contains LOS, which can be seen in the θ-polarized EPD in Fig. 4(a) as peaks in the angle range of 10° to 20° above horizontal plane. The LOS components with high elevation angles make the main lobe of the distribution wider also in the highway macrocell measurements. In the urban outdoor case the EPD becomes asymmetrical and more power is received at high elevation angles when the BS antenna is raised above the rooftop level. The negative slope of the EPD changes hardly at all. For large antenna heights also the XPR decreases for increasing elevation angle. In the urban macrocell case the XPR is approximately 0 dB for elevation angles above 60°. In the indoor picocell and outdoor–indoor cases the received power outside the main lobe is notably higher than in the outdoor measurements, most likely due to reflections from the ceiling. Similarly, the effect of the car can be seen as distortions in the EPD of the highway macrocell.

The elevation power distribution is described by the median elevation angle (M_θ), mean elevation angle ($\bar{\theta}$), rms elevation spread (σ_θ), defined as:

$$M_\theta, \text{ so that } \int_{-\pi/2}^{M_\theta} p(\theta)\cos\theta d\theta = \frac{1}{2} \tag{6}$$

$$\bar{\theta} = \int_{-\pi/2}^{\pi/2} \theta p(\theta)\cos\theta d\theta \tag{7}$$

$$\sigma_\theta = \int_{-\pi/2}^{\pi/2} \left[\theta - \bar{\theta}\right]^2 p(\theta)\cos\theta d\theta \tag{8}$$

where $p(\theta)$ is either $p_\theta(\theta)$ or $p_\phi(\theta)$. The parameters of the measured EPDs of all environments are presented in Table 3, from which the following observations can be made:

1) The rms elevation angle spread is larger for horizontal polarization in all environments.

2) In all outdoor environments the mean elevation angle is higher for horizontal polarization. In indoor picocell the situation is the opposite, due to the large portion of LOS measurements.

3) In all environments the mean elevation angle is higher than the median, i.e. the distribution is asymmetrical so that the spread is larger for high elevation angles than for low angles.

4) In urban environment the mean and median elevation angle, as well as the elevation spread, increase when the BS antenna height increases. A clear step in mean values can be seen between BS antenna heights 8 and 13 m in the urban microcell case.

C. Model for Elevation Power Distribution

It is proposed in [9] that the EPD has Gaussian shape in urban environment, when no LOS exists between MS and BS. However, as was observed in the previous section, the distribution is often not symmetrical about its peak value, but it decreases more rapidly on the negative side. Particularly this seems to be the case for BS antenna heights larger than 10 m, which is common for outdoor base stations also in urban environments. Fig. 5 presents the measured EPD for θ-polarization in urban macrocell environment together with two best-fit distribution functions:

1) Gaussian function:

$$p(\theta) = A_1 \exp\left[-\frac{(\theta-\theta_0)^2}{2\sigma^2}\right], \qquad \theta \in \left[-\frac{\pi}{2}, \frac{\pi}{2}\right] \tag{9}$$

2) General double exponential function[3]*:*

$$p(\theta) = \begin{cases} A_2 \exp\left[-\dfrac{\sqrt{2}|\theta-\theta_0|}{\sigma^-}\right], & \theta \in \left[-\dfrac{\pi}{2}, \theta_0\right] \\ A_2 \exp\left[-\dfrac{\sqrt{2}|\theta-\theta_0|}{\sigma^+}\right], & \theta \in \left[\theta_0, \dfrac{\pi}{2}\right] \end{cases} \tag{10}$$

In Eqs. (9,10) $p(\theta)$ is either $p_\theta(\theta)$ or $p_\phi(\theta)$, θ_0 is the peak elevation angle, and parameters σ, σ^-, and σ^+ control the spread of the functions. Coefficients A_1 and A_2 are set so that (1) is satisfied.

As can be seen in Fig. 5, in the case of an asymmetrical EPD the fitted symmetrical Gaussian function ($\theta_0 = 5.0°, \sigma = 7.6°$) does not give an accurate description of the EPD. Instead, the fitted general double exponential function ($\theta_0 = 2.2°, \sigma^- = 3.9°, \sigma^+ = 17.8°$) gives an accurate match with measured data for values larger than 0.7 % of the peak value. In order to find a representative statistical model for the elevation power distribution, and to study the effect of the model on the obtained mean effective gain of a mobile antenna, we fitted the measured power distributions in each environment to both model functions, by minimizing the squared approximation error (*SAE*) of the fitted curves, defined as:

$$SAE = \int_{-\pi/2}^{\pi/2} \left[p_{fit}(\theta) - p_{meas}(\theta)\right]^2 d\theta \tag{11}$$

where p_{fit} and p_{meas} are the modeled and measured distributions, respectively. Table 4 presents the best-fit parameters and approximation error of both functions. It can be seen that for most environments the SAE of the double exponential function is smaller than that of the Gaussian function, which indicates that the former yields better match with the experimental data. The difference is clearest for the cases with largest BS antenna heights (*urban macrocell, urban microcell with* h_{BS}=13 m).

[3]If the spread parameters σ^- and σ^+ are equal the double exponential function is called Laplacian function

In [9], Taga reported considerably larger values for the mean elevation angle and standard deviation of the Gaussian distribution derived from urban macrocell measurements in central Tokyo. However, the urban environment in Tokyo is quite different from that of Helsinki, which could explain the difference. Also the BS antenna height in his measurements was significantly larger (87 m) than in our measurements (27 m and 21 m), increasing the portion of power propagated over building rooftops.

D. Cross Polarization Power Ratio

In the case of vertically polarized transmission, the XPR is defined as the power ratio of θ- and ϕ-polarized components of the mean incident field. The XPR was obtained from the measurement data as the ratio of the integrals of the mean relative incident power vs. elevation angle (see Table 1):

$$XPR = \frac{\oint P_{\theta}(\theta)d\theta}{\oint P_{\phi}(\theta)d\theta} \tag{12}$$

The resulting XPR in each radio environment is shown in Table 3. The highest XPR values are obtained in the urban microcell environment; the XPR is approximately 11 dB for all BS antenna heights. XPR is close to 11 dB also in the outdoor-indoor case. Instead, for the indoor picocell, urban macrocell, and highway macrocell cases the XPR is close to 7 dB. In the existing literature few measurements of the XPR at the mobile station have been reported. In measurements presented in [21], the median "cross-polarization coupling", which is equal to the reciprocal of the XPR, was found to be as high as –2.5 dB inside and –3.5 dB outside houses in a residential area at 800 MHz. The values are clearly lower than what we measured at 2.15 GHz. According to measurements by Lee [22] and Taga [9], the XPR in urban macrocell environment is between 4 dB and 9 dB at 900 MHz. This is comparable to our measurements at 2.15 GHz, although the BS antenna height and BS–MS distance are considerably smaller. According to measurements by Lee and Yeh [22], the differences between the two cross coupling coefficients (VP→HP, HP→VP) are less than 2 dB. This indicates that XPR at the mobile station is comparable to the XPR at the base station. In [23] the mean XPR at the base station was found to be 7 dB in urban macrocell at 463 MHz when a vertically polarized antenna was used at the mobile station.

In our urban microcell and outdoor-indoor measurements the range was considerably smaller than in the above references. This would explain the higher obtained XPR values, under the assumption that the number of depolarizing reflections and diffractions on the propagation path increases when the separation between the

transmitter and receiver increases. In [24], XPR at the base station was found to be close to 10 dB in urban environment at 1800 MHz, and building penetration had minor influence on the XPR. In the highway macrocell measurements the close scattering from the bodywork of the car most probably decreases the XPR. Also in the indoor picocell measurements the low XPR value can be explained by the high number of close-proximity scatterers around the mobile.

V. MEG Comparison of Handset Antennas

A. Evaluated Antenna Configurations

To evaluate MEG as a parameter describing the handset antenna performance we picked three typical handset antennas: a commercial *GSM1800* handset with an external meandered monopole antenna, and simulated meandered monopole (*MEMO*) and planar inverted patch (*PIFA*) antennas attached to a handset model. In addition, we took an omnidirectional *discone* antenna for reference. We measured the 3-D gain patterns of the *discone* antenna and the *GSM1800* handset in an anechoic chamber with a grid of 10° in both elevation and azimuth. The measurement frequency was 2154 MHz for the *discone* and 1747 MHz for the *GSM1800* handset. Although the power distributions were obtained from measurements at 2154 MHz carrier frequency, they can be assumed valid also at 1800 MHz frequency range; the frequency difference is so small that the same propagation mechanisms are effective for waves at both frequencies. The *discone* was measured in free space only, while the *GSM1800* handset was measured both in free space and beside a model of human head and shoulders. In free space the handset was oriented vertically, but when placed beside the model it was tilted 60° degrees from vertical to correspond to a natural usage position. The handset touched the ear of the model. The used model was Torso Phantom V2.0 by Schmidt & Partner Engineering AG, and it was filled with brain-simulating liquid.

We simulated the 3-D gain patterns of the *MEMO* and *PIFA* by using a commercial FDTD program (XFDTD, version 5.1 Bio-Pro by Remcom, Inc.). Both antennas were attached to the top of a metallic chassis acting as the body of a mobile phone. The simulations were performed both in free space and beside a head model. The simulation frequency was 2154 MHz. In free space the phone chassis were oriented vertically. Beside the head, they were oriented according to the intended use position specified by CENELEC [25]. The phone was tilted 74° from vertical and 10° from the ear towards the cheek, as described in [26]. A distance of 5 mm was left between the head and phone chassis, corresponding to the actual position of the metallic chassis of a mobile phone. The

used head model was an FDTD mesh with 2.5 mm voxel resolution remeshed from a standard human head and shoulders model obtained from the software provider.

In both the measurements and simulations the head model was in upright position, and the nose pointed towards positive *y*-axis (see Fig. 1). The patterns were measured and simulated for the handset placed on both right and left side of the head, i.e. on the positive and negative *x*-axis sides, respectively. The horizontal (*xy*-plane) and vertical (*xz*-plane) cuts of the power gain patterns of all antenna configurations are presented in Fig. 6.

B. Mean Effective Gains of Antennas

We computed the MEGs of all evaluated antenna configurations using [9, Eq. (6)]. The distribution of the incident power was assumed uniform in azimuth. As the power distribution in elevation and cross polarization power ratio we used the data obtained from the experiments and presented in Section IV. Fig. 7 shows the MEG of each antenna configuration in all radio environments, together with the average MEG and the total antenna efficiency. Table 5 presents the average MEG, maximum gain, total antenna efficiency, and the cross-polarization discrimination (XPD) of each configuration. The cross-polarization discrimination is given by:

$$XPD = \frac{\int_0^{2\pi}\int_{-\pi/2}^{\pi/2} G_\theta(\theta,\phi)\cos\theta d\theta d\phi}{\int_0^{2\pi}\int_{-\pi/2}^{\pi/2} G_\phi(\theta,\phi)\cos\theta d\theta d\phi} \tag{13}$$

The total antenna efficiency (including the dielectric losses due to the head model) is obtained by:

$$\eta_{\text{tot}} = \frac{1}{4\pi}\int_0^{2\pi}\int_{-\pi/2}^{\pi/2}\left[G_\theta(\theta,\phi)+G_\phi(\theta,\phi)\right]\cos\theta d\theta d\phi \tag{14}$$

The reference level in the gain measurement of the *GSM1800* handset was the nominal maximum transmission power. Note that the MEG of an antenna in an artificial isotropic environment – i.e. for $p_\theta(\theta,\phi) = p_\phi(\theta,\phi) = \frac{1}{4\pi}$, $XPR = 1$ – is equal to the total antenna efficiency divided by two. Based on Table 5, no direct connection can be found between the MEG of an antenna configuration and its total efficiency or gain. Furthermore, it turned out that in most cases the differences in the MEG values could not be predicted directly

by analyzing the plane cuts of the radiation pattern. Only clearly negative XPD with dominating ϕ polarization predicted low MEG values.

Fig. 7 shows that the differences in MEG are clearly larger between antennas than between radio environments. This is understandable, since in all environments most of the power is received at small positive elevation angles (see Fig. 4). In effect, the XPR seems to explain most of the environmental dependence of the MEG, as will be presented below. The reference *discone* has by far the highest MEG: close to 0 dBi in all environments. This is due to its omnidirectional radiation pattern, high efficiency, and high cross-polarization discrimination. It should be noted that also the *MEMO* and *PIFA* have high efficiency in free space, but still their MEGs are significantly lower: of the order of −5 dBi.

When placed beside the head model, the total efficiency of the *MEMO* drops by 5.9/4.6 dB, depending on the side of the head (R/L). At the same time, the average MEG drops by 2.2/4.7 dB. Fig. 6 (c) shows that the θ-polarized pattern of the *MEMO* in free space has a minimum in the horizontal plane. Instead, beside the head the maximum of the θ-polarized pattern is produced at the horizontal plane. On the right side of the head θ polarization dominates, which partly compensates for the decreased efficiency. For *MEMO*, the difference in MEGs on the two sides of the head is 2.5 dB. For *PIFA,* the total antenna efficiency drops by 3.1/2.4 dB when placed beside the head, and the MEG drops on average by 2.7/3.0 dB.

The average MEG of the measured *GSM1800* handset increases by 1.3 dB when the handset is placed on the left side of the head of the human body model, although the total efficiency drops by 3.3 dB from the free space value. On the right side of the head the average MEG is 4.5 dB lower than on the left side, although the total efficiency is 0.3 dB higher. The maximum gain of the antenna configuration is almost the same on both sides of the head (note that in free space the gain is lower). The result clearly indicates that maximum gain or total efficiency of an antenna is not enough to describe its performance in practical environments.

When any of the two simulated antennas is placed on the left side of the head, the highest MEG values are obtained in environments with lowest XPR (see Fig. 7). The behavior is partly explained by the XPD values of the antenna configurations, which are lower on the left side than the right (see Table 5). The opposite happens for the measured *GSM1800*, which had the antenna located on the opposite corner of the handset. The highest variation of MEG values between different environments is obtained for antenna configurations with negative XPDs.

It has been observed also previously [27] that the MEG of a handset antenna depends on which side of the head the user holds the handset. In [27], the average user influence at 1800 MHz frequency was found to be a loss of 10 dB for a helical antenna, and 3 dB for a patch antenna. In our analysis the average decrease in MEG due to the user was 0.8 dB, 3.3 dB and 2.8 dB for the measured *GSM1800* and the simulated *MEMO* and *PIFA*, respectively. However, we only modeled the head of the user (also the shoulders for the measured handset), and not the hand or full body, which partly explains the difference.

C. *Effect of Model Distribution on MEG*

In order to evaluate the two models for the elevation power distribution (see Sec. IV.C), we repeated the MEG computation for the same antennas using the model distributions, fitted separately for each environment using parameters given in Table 4. For XPR, the values obtained directly from measurements (presented in Table 3) were used. The average differences between the MEGs obtained for the measured and the two modeled EPDs are plotted in Figs. 8 and 9. The MEG errors of both models are small, less than 0.5 dB for the Gaussian distribution, and less than 0.1 dB for the General double exponential distribution. The differences between antennas (Fig. 8) are larger than the differences between the environments (Fig. 9). This can be understood based on the results shown in the previous section, showing that the environment type has quite small effect on the obtained MEG.

VI. CONCLUSIONS

We applied a novel technique for measuring the angular distribution and cross-polarization ratio of the incident power at the mobile station in different types of propagation environments. This information is needed in the evaluation of mobile handset antenna performance in realistic operating environments. The results show that in NLOS situations the power distribution in elevation has a shape of a double-sided exponential function, with different slopes on the negative and positive sides of the peak. The slopes and the peak elevation angle depend on the environment and base station antenna height. We noticed that the distribution becomes asymmetrical when the antenna is raised above the rooftop level in urban environment. With lower BS antenna heights the power is concentrated only slightly above the horizontal plane.

The measured cross-polarization power ratio was smallest in indoor picocell and urban macrocell environments, of the order of 7 dB. A similar value was obtained also when the mobile antenna was placed inside a person car

in measurements on a highway. In urban microcell and outdoor-indoor measurements with relatively short ranges the XPR was fairly large, approximately 11 dB.

We applied the experimental data for analysis of the mean effective gain of several practical handset antennas. The MEG values varied from approximately −5 dBi in free space to less than −11 dBi beside the head model. These values are considerably lower than the 0 dBi typically used in system specifications, e.g. [28]. The result shows that considering only the maximum gain or total efficiency of the antenna is not enough to describe its performance in practical operating conditions. In all measured environments the cross polarization coupling was fairly small, indicating that the polarization of a handset antenna should be matched to that of the BS antenna, to obtain best performance. However, the polarization of the antenna is sensitive to the usage position of the handset, which should be considered in antenna design.

For most antennas the environment type has little effect on the MEG, but clear differences exist between antennas. The MEG also depends on which side of the head the user holds the handset. Errors in MEG values caused by using any of the two power distribution models instead of the measured power distributions were small: on average less than 0.5 dB for the Gaussian distribution, and less than 0.1 dB for the General double exponential distribution.

In this contribution we only considered the mean value of the effective gain of a handset antenna. However, it is also important to know the probability levels of which a certain portion of the total incident power is received. The measurements described in this paper allow the analysis of such instantaneous reception efficiency of a handset, as well as more sophisticated analysis like estimation of polarization diversity gain, which are important issues for further studies.

VII. Acknowledgements

The authors wish to thank Martti Toikka, Lasse Vuokko, Jani Ollikainen, Pasi Suvikunnas, and Eero Rinne for their help in carrying out the radio channel measurements. The work was partially funded by the National Technology Agency of Finland (TEKES), and the Graduate School in Electronics, Telecommunications and Automation (GETA). Financial support from the Finnish Society of Electronics Engineers, HPY Foundation, Nokia Foundation, and Wihuri Foundation is also gratefully acknowledged.

VIII. REFERENCES

[1] J. B. Andersen and F. Hansen, "Antennas for VHF/UHF Personal Radio: A Theoretical and Experimental Study of Characteristics and Performance," *IEEE Transactions on Vehicular Technology*, vol. 26, no. 4, pp. 349–357, November 1977.

[2] H. Arai, N. Igi, and H. Hanaoka, "Antenna-Gain Measurement of Handheld Terminals at 900 MHz," *IEEE Transactions on Vehicular Technology,* vol. 46, no. 3, pp. 537-543, August 1997.

[3] I. Z. Kovács, P. C. F. Eggers, and K. Olesen, "Comparison of Mean Effective Gains of different DCS1800 handset antennas in urban and suburban environments", *Proc. IEEE 48th Vehicular Technology Conference (VTC98),* Ottawa, Ontario, Canada, May 18-21, 1998, pp. 1974-1978.

[4] K. Sulonen, K. Kalliola, and P. Vainikainen, "Comparison of Evaluation Methods for Mobile Handset Antennas," *Proceedings of Millennium Conference on Antennas & Propagation (AP2000),* Davos, Switzerland, April 9-14, 2000, CD-ROM SP-444 (ISBN 92-9092-776-3), paper p0870.pdf.

[5] B. M. Green and M. A. Jensen, "Diversity Performance of Dual-Antenna Handsets Near Operator Tissue," *IEEE Transactions on Vehicular Technology*, vol. 48, no. 7, pp. 1017-1024, July 2000.

[6] G. F. Pedersen and J. Bach Andersen, "Handset Antennas for Mobile Communications: Integration, Diversity, and Performance," Chapter 5 in *Review of Radio Science 1996-1999,* editor W.R. Stone, Oxford, Oxford University Press, 1999, 970 p.

[7] H. Arai, *Measurement of Mobile Antenna Systems,* Boston, Artech House, 2001, 214 p.

[8] B. G. H. Olsson, "Simplistic Field Distribution Estimation of a Scattered Field Measurement Room," *Proc. IEEE 51st Vehicular Technology Conference (VTC2000-Spring),* Tokyo, Japan, 15-18 May, 2000, vol. 3, pp. 2482-2486.

[9] T. Taga, "Analysis for mean effective gain of mobile antennas in land mobile radio environments," *IEEE Transactions on Vehicular Technology*, vol. 39, no. 2, pp. 117-131, May 1990.

[10] M. B. Knudsen, G. F. Pedersen, B. G. H. Olsson, K. Olesen, and S.-Å. A. Larsson, "Validation of Handset Antenna Test Methods," *Proc. IEEE 52nd Vehicular Technology Conference (VTC2000-Fall),* Boston, MA, USA, 24-28 September, 2000, vol. 4, pp. 1669-1676.

[11] A. Kuchar, J.-P. Rossi, and E. Bonek, "Directional Macro-Cell Channel Characterization from Urban Measurements," *IEEE Transactions on Antennas and Propagation,* vol. 48, no. 2, pp. 137-146, February 2000.

[12] H. Laitinen, K. Kalliola, and P. Vainikainen, "Angular Signal Distribution and Cross-Polarization Power Ratio Seen by a Mobile Receiver at 2.15 GHz," *Proceedings of Millennium Conference on Antennas & Propagation (AP2000),* Davos, Switzerland, April 9-14, 2000, CD-ROM SP-444 (ISBN 92-9092-776-3), paper p1133.pdf.

[13] S. Qu and T. Yeap, "A three-dimensional scattering model for fading channels in land mobile environment," *IEEE Transactions on Vehicular Technology*, vol. 48, no. 3, May 1999, pp. 765-781.

[14] K. Kalliola, H. Laitinen, L. I. Vaskelainen, and P. Vainikainen, "Real-time 3D Spatial-Temporal Dual-polarized Measurement of Wideband Radio Channel at Mobile Station," *IEEE Transactions on Instrumentation and Measurement*, vol. 49, no. 2, pp. 439-448, April 2000.

[15] R. H. Clarke, "3-D Mobile Radio Channel Statistics," *IEEE Transactions on Vehicular Technology*, vol. 46, no. 3, August 1997, pp. 798-799.

[16] R. H. Clarke, "A statistical theory of mobile radio reception," *Bell. Syst. Tech. J.*, vol. 47, July/Aug. 1968, pp. 957-1000.

[17] T. Aulin, "A Modified Model for the Fading Signal at a Mobile Radio Channel," *IEEE Transactions on Vehicular Technology*, vol. 28, no. 3, pp. 182-203, August 1979.

[18] J. Kivinen, T. Korhonen, P. Aikio, R. Gruber, P. Vainikainen, S.-G. Häggman, "Wideband Radio Channel Measurement System at 2 GHz", *IEEE Transactions on Instrumentation and Measurement*, vol. 48, no. 1, February 1999, pp. 39-44.

[19] J. Laurila, K. Kalliola, M. Toeltsch, K. Hugl, P. Vainikainen, and E. Bonek, "Wideband 3-D Characterization of Mobile Radio Channels in Urban Environment", *To be Published in IEEE Transactions on Antennas and Propagation*, 2001.

[20] W. C.-Y. Lee and R. H. Brandt, "The Elevation angle of Mobile Radio Signal Arrival," *IEEE Transactions on Communications*, vol. COM-21, no. 11, November 1973, pp. 1194–1197.

[21] D. C. Cox, R. R. Murray, H. W. Arnold, A. W. Norris, and M. F. Wazowicz, "Cross-Polarization Coupling Measured for 800 MHz Radio Transmission In and Around Houses and Large Buildings," *IEEE Transactions on Antennas and Propagation*, vol. 34, no. 1, January 1986, pp. 83–87.

[22] W. C.-Y. Lee and Y.S. Yeh, "Polarization Diversity System for Mobile Radio," *IEEE Transactions on Communications*, vol. COM-20, no. 5, October 1972, pp. 912–923.

[23] R. Vaughan, "Polarization Diversity in Mobile Communications," *IEEE Transactions on Vehicular Technology*, vol. 39, no. 3, August 1990, pp. 177–186.

[24] P. C. F. Eggers, I. Z.Kovács, and K. Olesen, "Penetration effects on XPD with GSM1800 handset antennas, relevant for BS polarization diversity for indoor coverage," *Proc. IEEE 48th Vehicular Technology Conference (VTC98),* Ottawa, Ontario, Canada, May 18-21, 1998, pp. 1959-1963.

[25] European specification (ES 59005), *Considerations for the Evaluation of Human Exposure to Electromagnetic Fields (EMFs) from Mobile Telecommunication Equipment (MTE) in the Frequency Range 30 MHz - 6 GHz*, Brussels, Belgium, CENELEC, October 1998, 81 p.

[26] J. T. Rowley and R. B. Waterhouse, "Performance of Shorted Microstrip Patch Antennas for Mobile Communications Handsets at 1800 MHz," *IEEE Transactions on Antennas and Propagation*, vol. 47, no. 5, May 1999, pp. 815-822.

[27] G. F. Pedersen, J. Ø. Nielsen, K. Olesen, and I. Z. Kovács, "Measured Variation in Performance of Handheld Antennas for a Large Number of Test Persons," *Proc. IEEE 48th Vehicular Technology Conference (VTC98),* Ottawa, Ontario, Canada, May 18-21, 1998, pp. 505-509.

[28] ETSI Technical Report TR 101 112 V3.2.0 (1998-04), *Universal Mobile Telecommunications System (UMTS); Selection procedures for the choice of radio transmission technologies of the UMTS (UMTS 30.03 version 3.2.0)*, European Telecommunications Standards Institute, 1998, 84 p.

TABLES

Table 1. Definitions of angular power distributions. Subscripts denote polarizations.

Definition	Azimuth	Elevation
Instantaneous power as a function of incidence angle.	$P_{\theta,i}(\phi)=\int_{\tau}\int_{\theta}\left\|h_{\theta,i}(\theta,\phi,\tau)\right\|^2\cos\theta d\theta d\tau$ $P_{\phi,i}(\phi)=\int_{\tau}\int_{\theta}\left\|h_{\phi,i}(\theta,\phi,\tau)\right\|^2\cos\theta d\theta d\tau$	$P_{\theta,i}(\theta)=\int_{\tau}\int_{\phi}\left\|h_{\theta,i}(\theta,\phi,\tau)\right\|^2 d\phi d\tau$ $P_{\phi,i}(\theta)=\int_{\tau}\int_{\phi}\left\|h_{\phi,i}(\theta,\phi,\tau)\right\|^2 d\phi d\tau$
Mean relative power as a function of incidence angle.	$P_{\theta}(\phi)=\frac{1}{N}\sum_{i=1}^{N}\frac{P_{\theta,i}(\phi)}{\oint\left[P_{\theta,i}(\phi)+P_{\phi,i}(\phi)\right]d\phi}$ $P_{\phi}(\phi)=\frac{1}{N}\sum_{i=1}^{N}\frac{P_{\phi,i}(\phi)}{\oint\left[P_{\theta,i}(\phi)+P_{\phi,i}(\phi)\right]d\phi}$	$P_{\theta}(\theta)=\frac{1}{N}\sum_{i=1}^{N}\frac{P_{\theta,i}(\theta)}{\oint\left[P_{\theta,i}(\theta)+P_{\phi,i}(\theta)\right]\cos\theta d\theta}$ $P_{\phi}(\theta)=\frac{1}{N}\sum_{i=1}^{N}\frac{P_{\phi,i}(\theta)}{\oint\left[P_{\theta,i}(\theta)+P_{\phi,i}(\theta)\right]\cos\theta d\theta}$
Power distributions in azimuth (APD) and elevation (EPD).	$p_{\theta}(\phi)=\frac{P_{\theta}(\phi)}{\oint P_{\theta}(\phi)d\phi}$ $p_{\phi}(\phi)=\frac{P_{\phi}(\phi)}{\oint P_{\phi}(\phi)d\phi}$	$p_{\theta}(\theta)=\frac{P_{\theta}(\theta)}{\oint P_{\theta}(\theta)\cos\theta d\theta}$ $p_{\phi}(\theta)=\frac{P_{\phi}(\theta)}{\oint P_{\phi}(\theta)\cos\theta d\theta}$

Table 2. Amount of collected data.

Environment	***Route length***	***Snapshots***	***LOS***	***NLOS***
Indoor picocell (Airport)	260 m	N = 9 800	40 %	60 %
Outdoor – Indoor (Office)	220 m	N = 8 300	0 %	100 %
Urban microcell (h_{BS} =3/8/13 m)	3×1200 m = 3600 m	3×51 000 N=153 000	22 %	78 %
Urban macrocell (h_{BS} = 21/27 m)	2560 m	N=100 600	4 %	96 %
Highway macrocell	2500 m	N = 47 600	25+45* %	30 %
TOTAL	**9140 m**	***N*=319 300**	**23 %**	**77 %**

*LOS obstructed by trees

Table 3. EPD parameters (p_θ / p_ϕ) and XPR.

Environment	M_θ	$\bar{\theta}$	σ_θ	*XPR*
Indoor picocell	2.1°/1.1°	3.8°/1.9°	8.7°/10.7°	7.0 dB
Outdoor – Indoor	–1.0°/ –0.9°	0.6°/1.8°	8.1°/14.6°	10.7 dB
Urban microcell:				
h_{BS} = 3 m	0.7°/1.5°	2.2°/3.5°	5.4°/7.8°	11.4 dB
h_{BS} = 8 m	1.3°/1.6°	2.4°/2.6°	6.2°/8.5°	11.4 dB
h_{BS} = 13 m	2.7°/3.1°	4.6°/5.7°	6.9°/9.9°	11.1 dB
Urban macrocell	7.2°/13.8°	11.2°/17.1°	11.9°/18.5°	7.3 dB
Highway macrocell	4.5°/6.4°	6.6°/10.9°	10.4°/14.5°	6.6 dB
Average of all environments	2.0°/3.7°	4.4°/7.5°	9.0°/14.7°	9.0 dB

Table 4. Best-fit parameters of EPD models (p_θ / p_ϕ).

	Gaussian function			*General double exponential function*			
Environment	θ_0 [°]	σ [°]	*SAE* [×1e^{-3}]	θ_0 [°]	σ^- [°]	σ^+ [°]	*SAE* [×1e^{-3}]
Indoor picocell	2.8/2.0	5.9/7.1	1.9/0.9	2.0/2.2	6.9/10.5	9.4/10.0	0.9/1.4
Outdoor – Indoor	–0.2/–0.2	3.9/5.8	1.4/3.0	–0.2/–0.2	5.4/8.1	5.5/8.3	0.5/1.6
Urban microcell:							
h_{BS} = 3 m	1.4/2.0	3.3/4.2	1.3/2.3	1.6/1.4	4.6/4.9	4.4/7.0	0.7/0.2
h_{BS} = 8 m	2.0/2.2	4.6/4.9	0.7/0.9	1.8/2.0	5.9/6.3	6.7/7.1	1.0/0.6
h_{BS} = 13 m	3.4/3.6	4.6/5.4	1.4/2.2	2.0/1.8	4.3/4.8	8.2/10.0	0.4/0.2
Urban macrocell	5.0/5.0	7.6/19.7	4.4/4.9	2.2/2.0	3.9/4.6	17.8/37.4	0.2/0.7
Highway macrocell	5.0/5.8	4.7/6.7	3.4/5.0	6.0/6.0	8.0/9.6	5.7/10.0	3.5/2.9
Average of all environments	2.6/3.6	5.0/7.3	1.5/2.5	1.6/1.8	5.5/7.4	8.6/13.7	0.2/0.6

Table 5. Evaluated antennas configurations.

	Antenna	*Tilt angle*[1]	η_{tot} [%]	G_{max} [dBi]	*XPD* [dB]	*MEG* [dBi]
MEASURED	Discone	0°	95	2.9	13.0	0.0
	GSM1800	0°	56	1.5	4.6	−8.5
	GSM1800 + torso R	60°	28	3.7	−5.8	−11.7
	GSM1800 + torso L	60°	26	4.0	−0.1	−7.2
SIMULATED	MEMO	0°	100	3.8	−0.7	−5.1
	MEMO+head R	74°	26	2.8	0.2	−7.3
	MEMO+head L	74°	35	3.3	−5.1	−9.8
	PIFA	0°	100	4.6	−0.2	−5.4
	PIFA+head R	74°	49	4.3	−3.0	−8.1
	PIFA+head L	74°	57	4.7	−5.6	−8.4

[1]from vertical

FIGURES

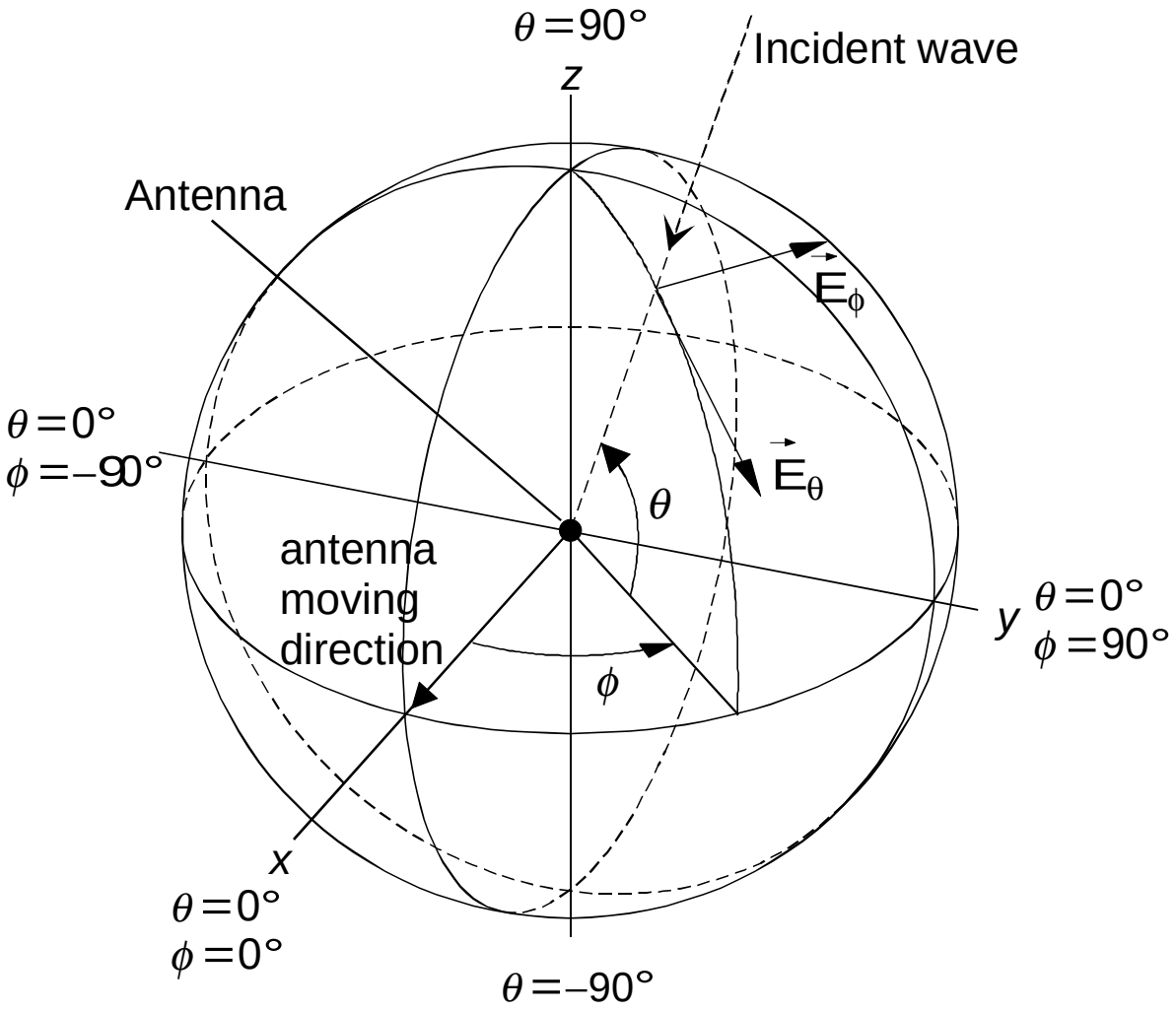

Figure 1. Spherical coordinate system.

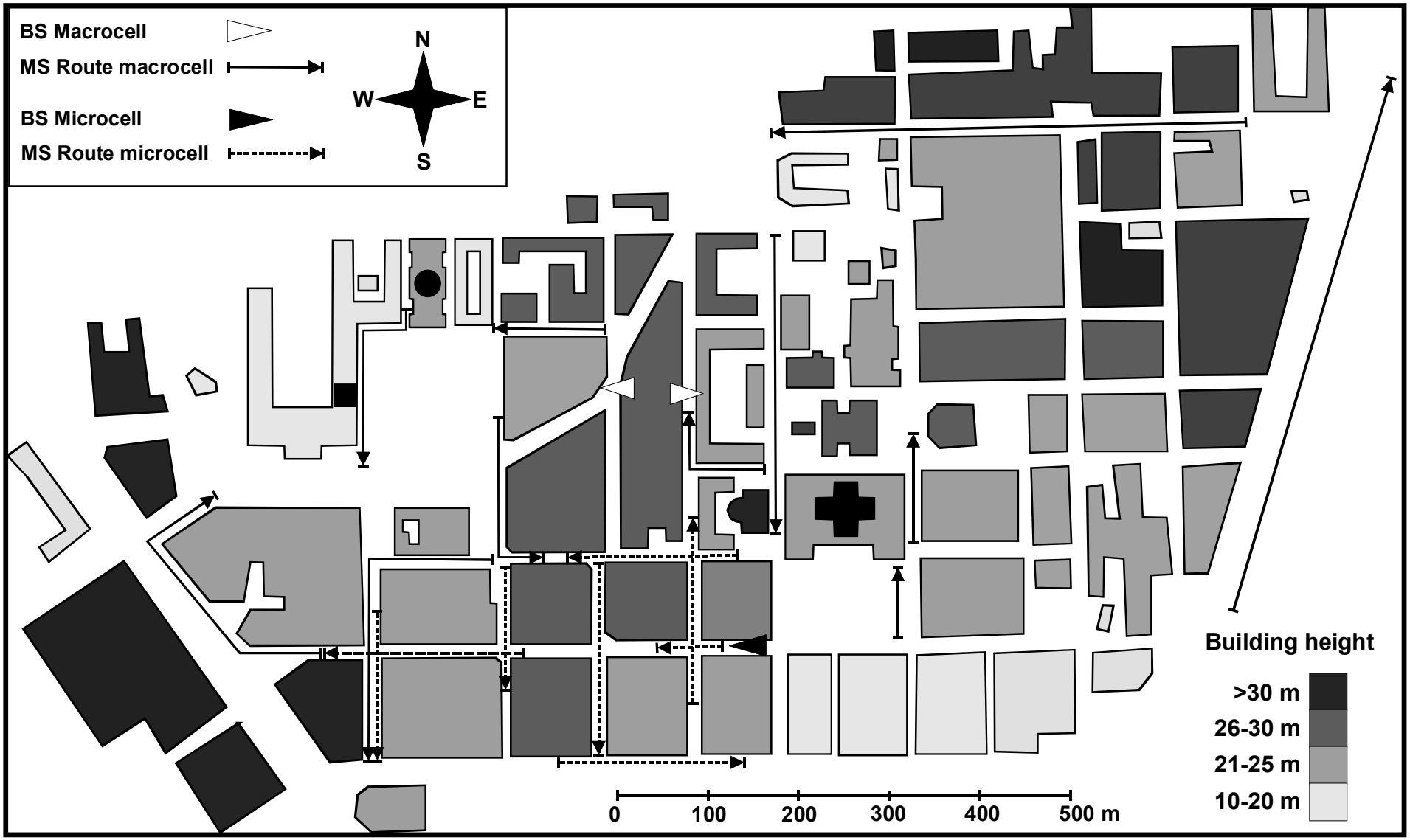

Figure 2. Measurement routes in the center of Helsinki.

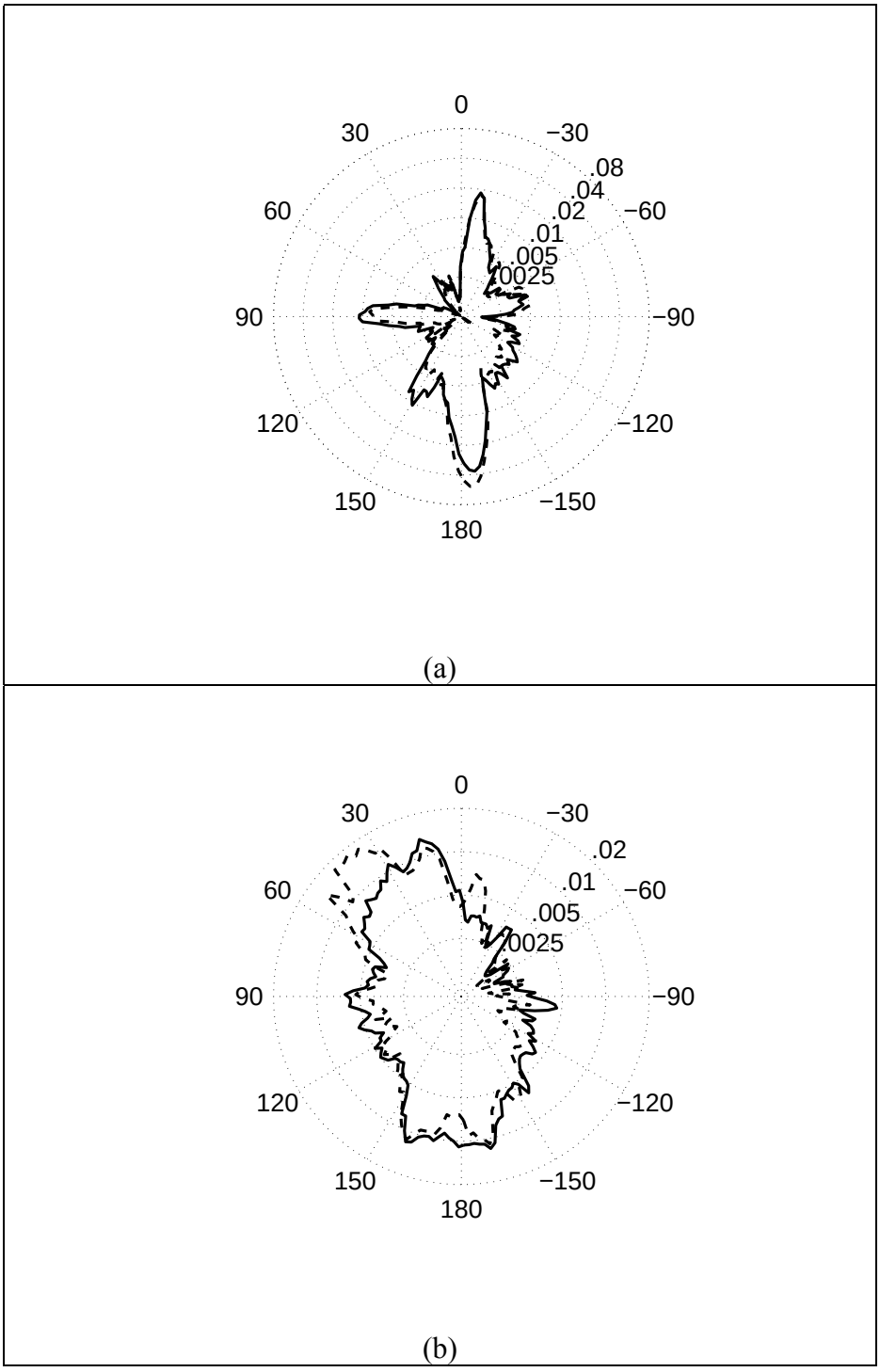

Figure 3. Mean azimuth power distributions. (a) Urban microcell, h_{BS} = 3 m. (b) Urban macrocell. Mobile moving direction is 0° (——— $p_\theta(\phi)$, – – – $p_\phi(\phi)$).

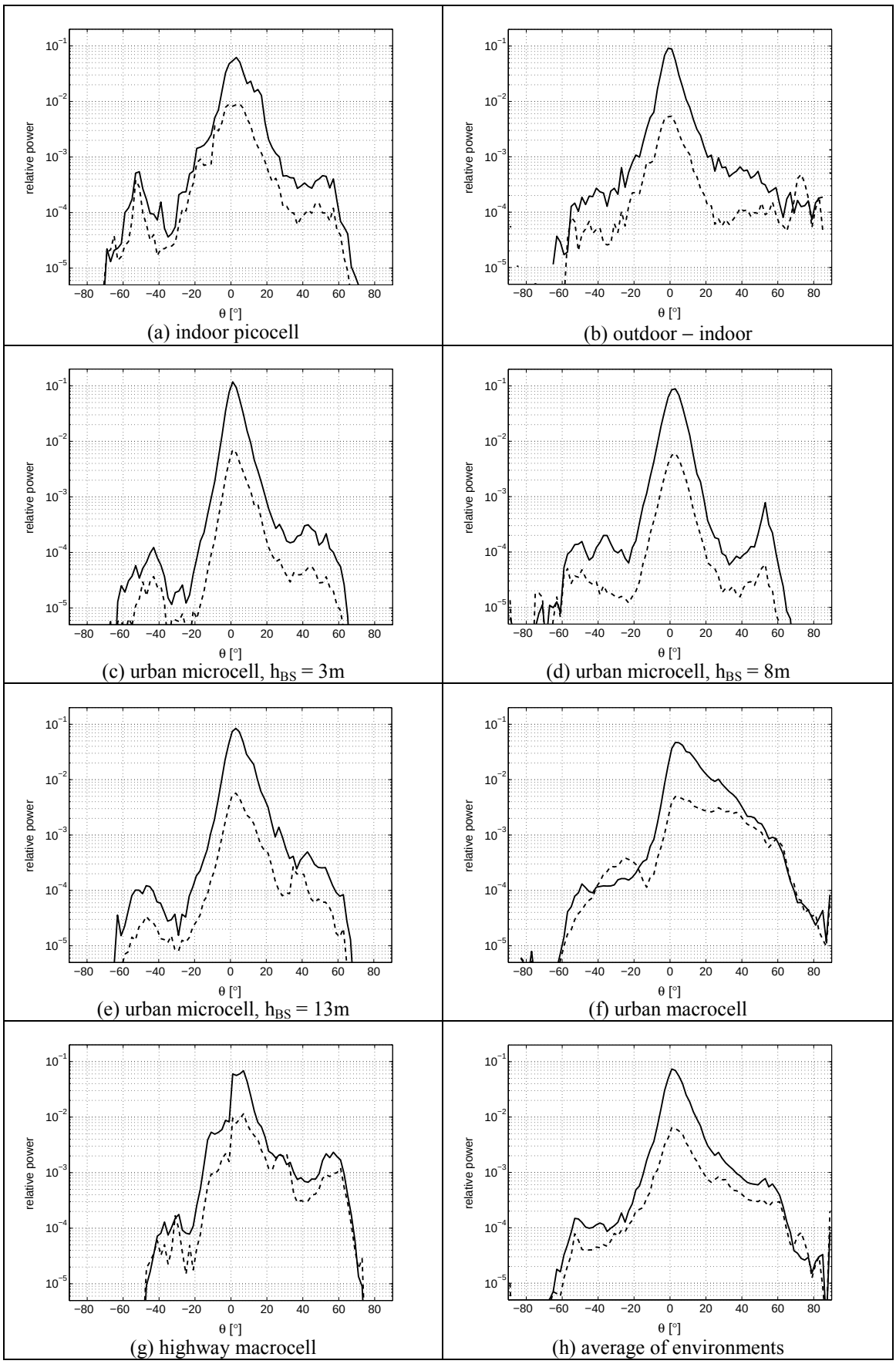

Figure 4. Mean relative power vs. elevation angle at mobile station in different radio environments (——— $P_\theta(\theta)$, – – – $P_\phi(\phi)$)

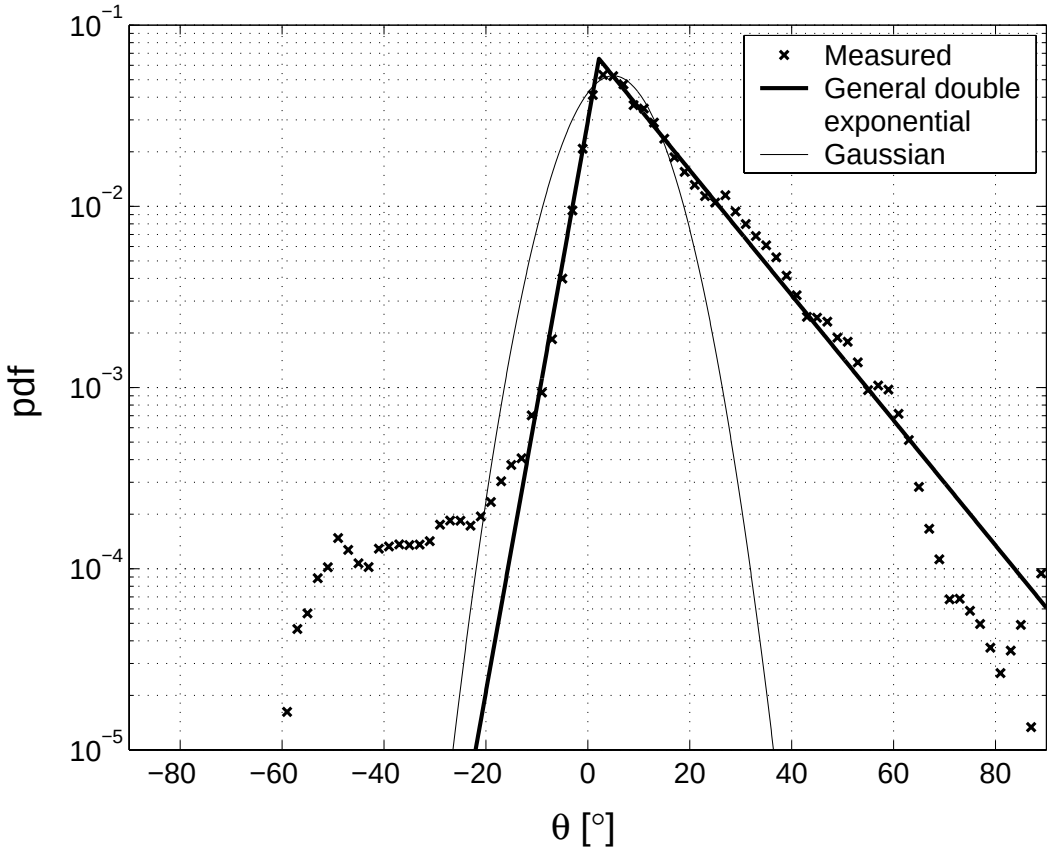

Figure 5. Example of two EPD models. Measurement data is from urban macrocell. θ polarization.

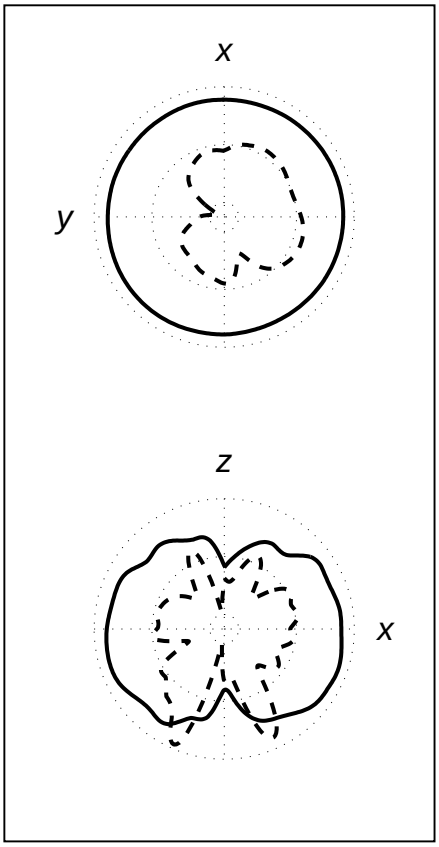

(a) Discone in free space

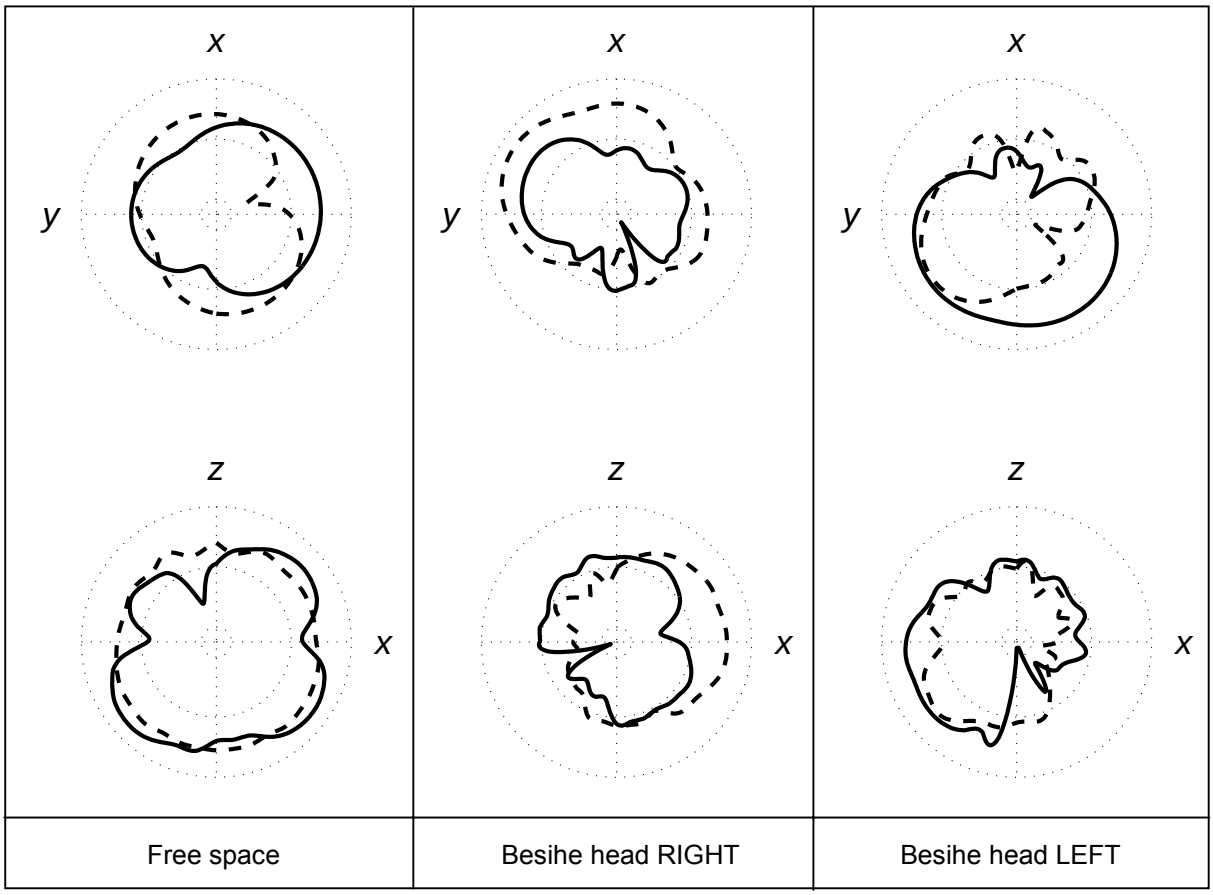

Free space	Besihe head RIGHT	Besihe head LEFT

(b) GSM1800

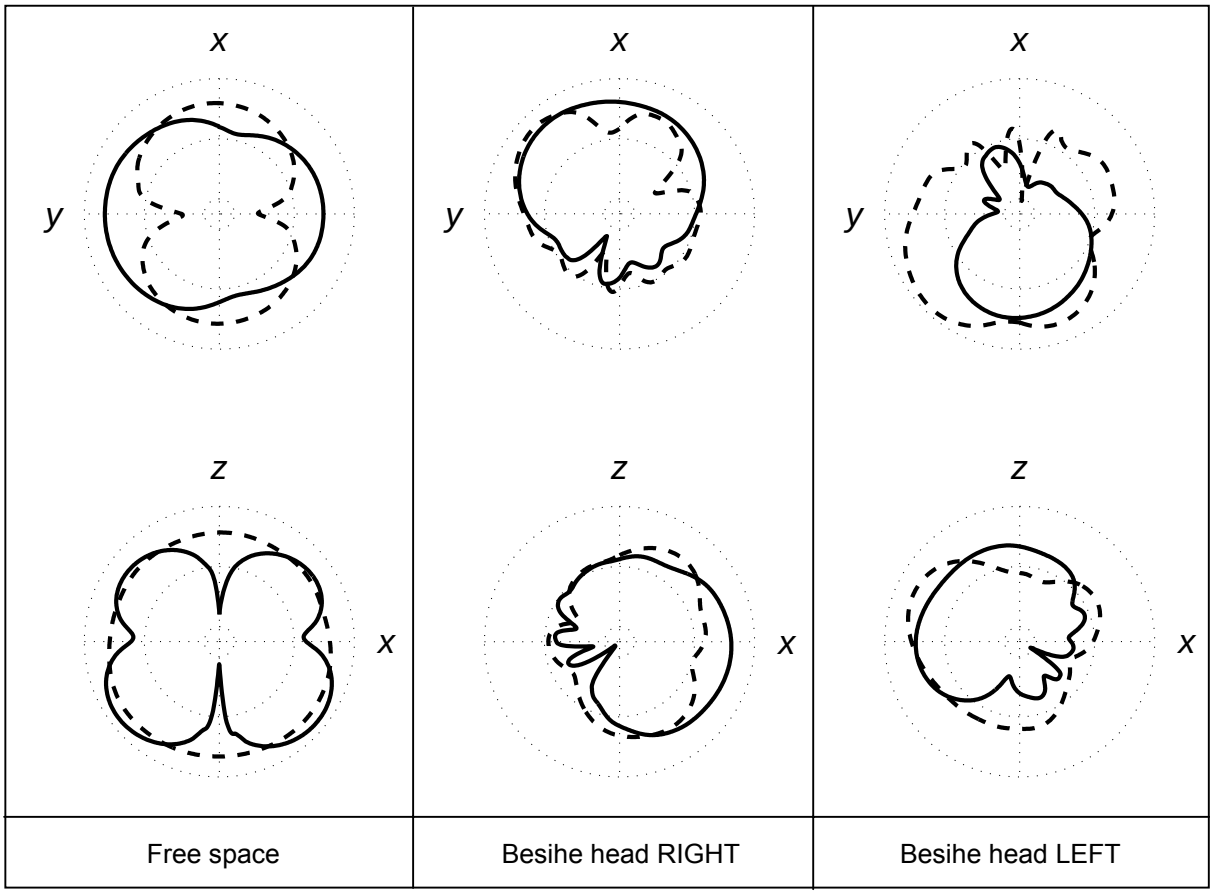

Free space	Besihe head RIGHT	Besihe head LEFT

(c) MEMO

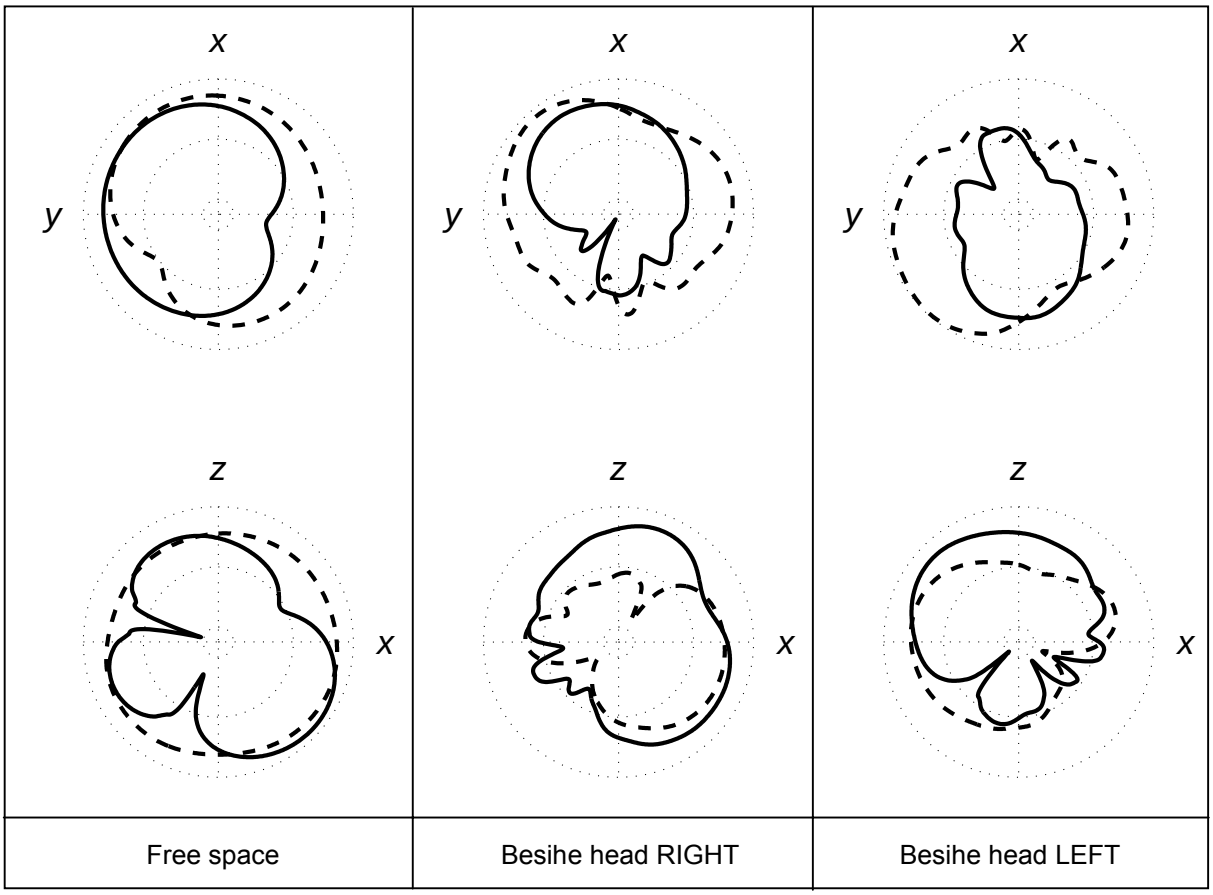

(d) PIFA

Figure 6. Gain patterns of evaluated antenna configurations. Top: horizontal plane cut. Bottom: vertical plane cut (—— θ polarization, – – – ϕ polarization). The dotted circles correspond to gain levels of +5, –15, and –35 dBi.

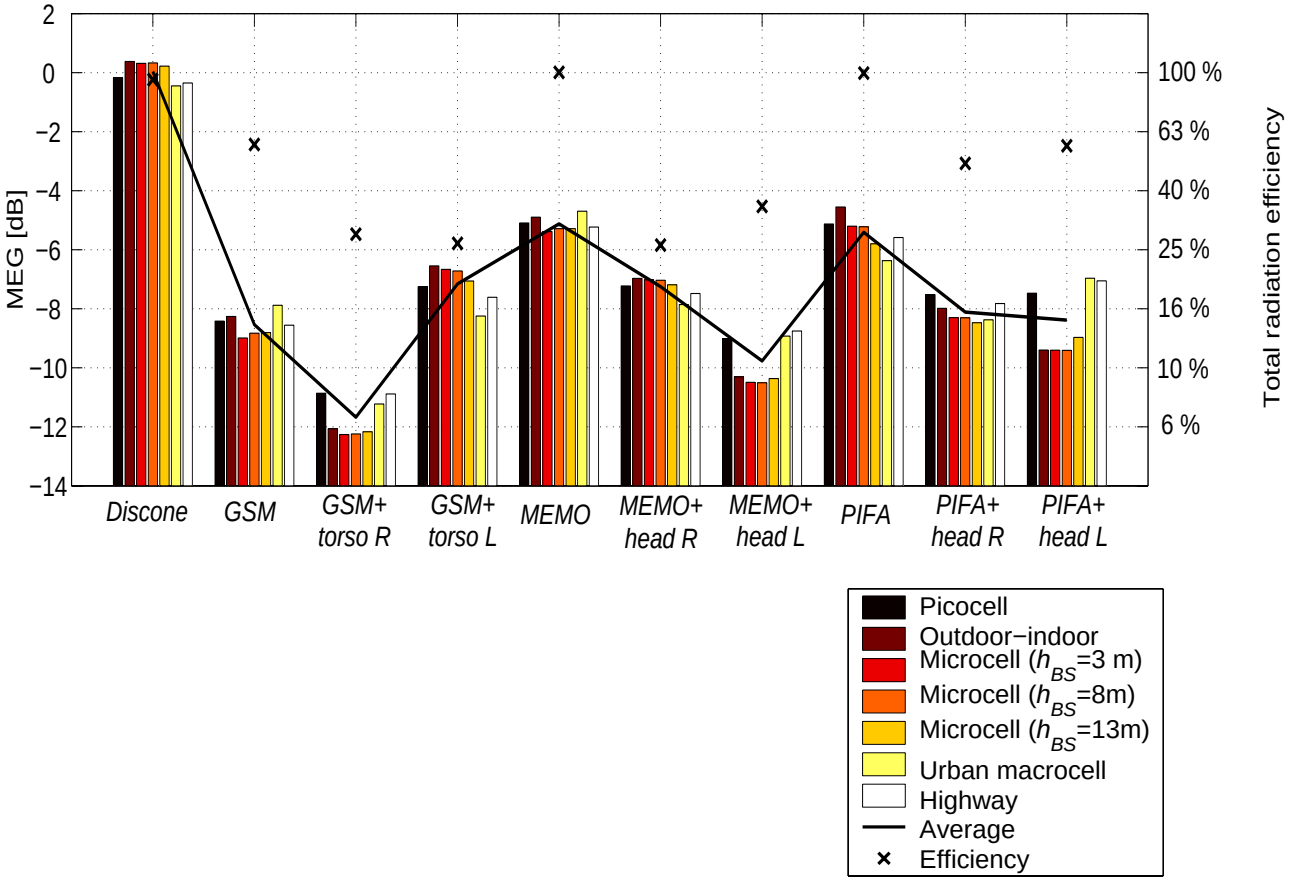

Figure 7. Mean effective gains of evaluated antennas.

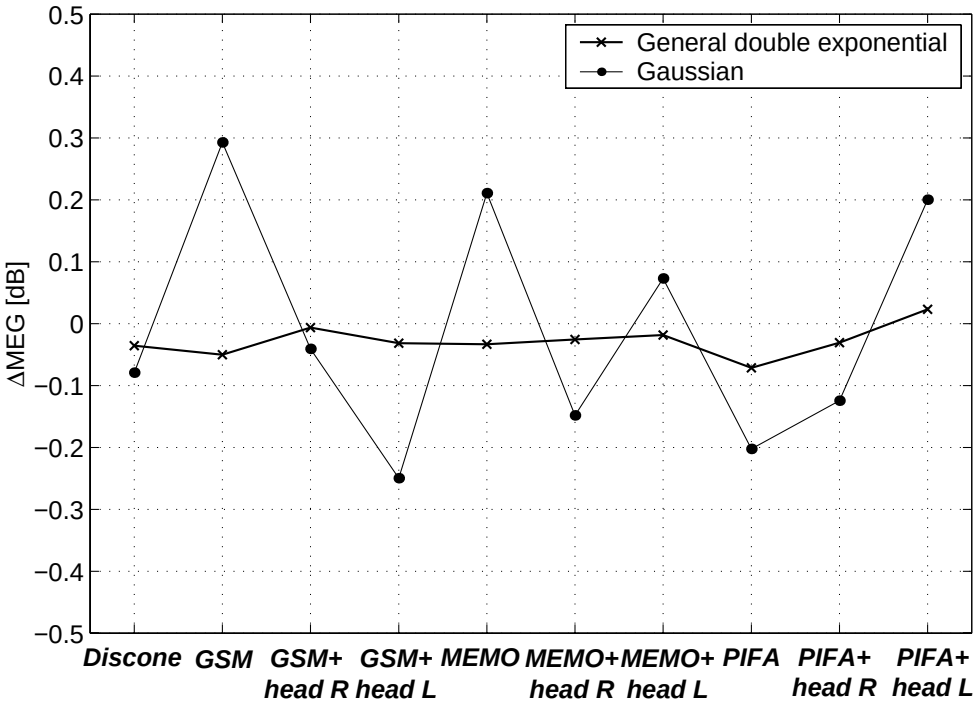

Figure 8. Difference of MEGs computed from measured and modeled EPDs. Average over environments.

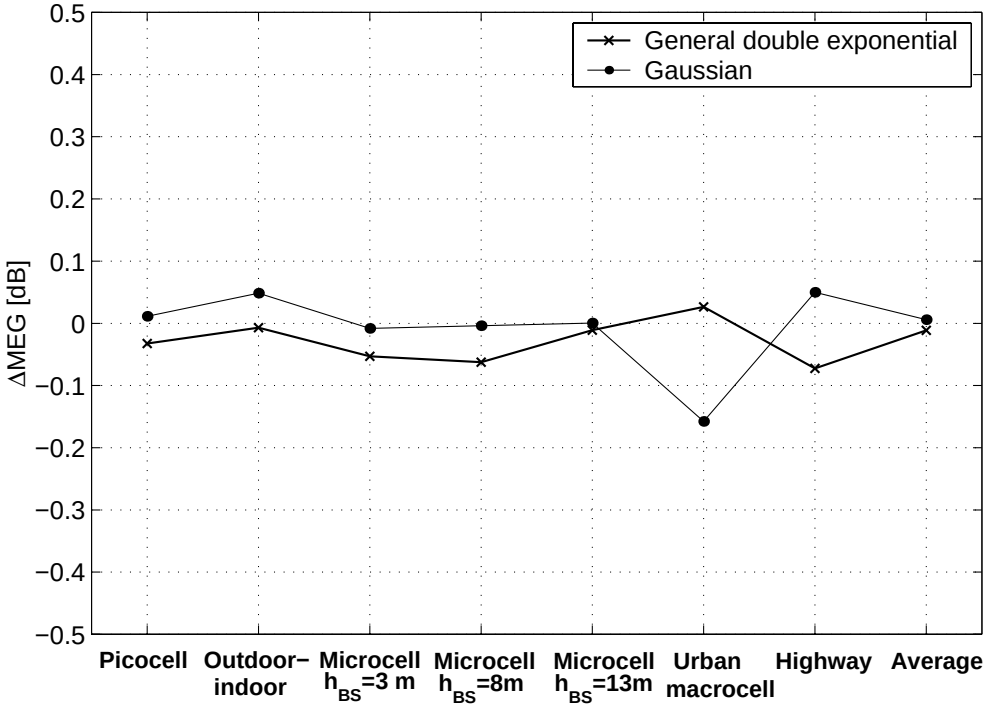

Figure 9. Difference of MEGs computed from measured and modeled EPDs. Average over antennas.